

Synthesis of quinoline functionalized fluorescent chemosensor for Cu (II), DFT studies and its application in imaging in living HEK 293 cells

Kajal Mal^a, Barnali Naskar^a, Tandrima Chaudhuri^b, Chandraday Prodhon^c, Sanchita Goswami^a, Keya Chaudhuri^c, Chhanda Mukhopadhyay^{a,*}

^a Department of Chemistry, University of Calcutta, 92 APC Road, Kolkata, 700009, India

^b Department of Chemistry, Dr. B. N. Dutta Smriti Mahavidyalaya, Burdwan, 713407, India

^c Molecular & Human Genetics Division, CSIR-Indian Institute of Chemical Biology, 4 Raja S.C. Mallick Road, Kolkata, 700032, India

ARTICLE INFO

Keywords:

Quinoline derivatives
Fluorescent sensor
Bivalent copper
DFT
Cell imaging experiment

ABSTRACT

New fluorescent probes having quinoline moiety have been successfully synthesized for the selective Cu²⁺ ions detection. These sensors show a favorable selectivity towards Cu²⁺ ion over a broad range of other common metal ions in DMSO/H₂O (2:8, v/v) HEPES buffer solution (pH = 7.4), leading to remarkable fluorescence on-off response with very low Limit of Detection (LOD) value. The robust nature of the probes was shown by the detection of Cu²⁺ even after repeated rounds of the experiment. Moreover, the probe can be used to detect Cu²⁺ in real water samples with a high precision and good accuracy. The recognition mechanism of one representative probe towards Cu²⁺ has been properly inspected in details by High Resolution Mass Spectrometry (HRMS) and density functional theory (DFT) calculations. Besides, fluorescence imaging studies in HEK 293 cells of that probe is also indicating that the probe is low cytotoxic and offers good photophysical properties, suggesting that this fluorescent chemosensor can be easily used to track Cu²⁺ ion in cells.

1. Introduction

The improvement of chemosensors via optical signal transduction has been of a great interest for the selective recognition of metal ions which can have incredible consequences on the environment as well as health of human [1]. Some essential metal ions, such as Na⁺, Ca²⁺, K⁺, Mg²⁺, Fe³⁺, Cu²⁺ and Zn²⁺ may affect biological processes like the conduction of impulses, nerve impulses, muscle contraction, ion-dependent establishment of electrochemical gradients across all the cell plasma membrane, muscle relaxation, cell function etc [2]. Among them, in human body copper is third (in abundance after iron and zinc) most essential metal trace element and plays a significant role in many lifecycle processes such as red blood cell formation, prosthetic group formation, bone formation, respiration etc [3,2,4]. Several research groups have attached the cellular toxicity of Cu²⁺ to serious diseases like Alzheimer's disease [5], familial amyotrophic lateral sclerosis [6], Indian childhood cirrhosis [7], prion disease [8], Wilson and Menkes diseases [9] which are all pathogenically connected with an intracellular deficiency and overload of copper. Monitoring of copper existing in biological resources is an important task all over the world because uptake of excessive copper ions may lead to damage of living organs such as kidney and liver [10]. In our modern society Cu²⁺ is

extensively used and it results copper a significant metal pollutant. According to the U.S. Environmental Protection Agency (EPA), the permissible level of copper in drinking water is 20 μM [11]. So the progress of a non-toxic small molecule-based signaling system which is reliable and Compatible for the recognition of Cu²⁺ in living species is a supreme important to us.

In recent years, designing of fluorescent sensors has emerged to be the most popular and significant approach for the detection of metal ions [12]. Even at very low concentration, Fluorescent based sensors can detect common metal ions and can serve up as agents for imaging. The added superiorities over other methods are operational simplicity, high sensitivity, easy operation, remarkable selectivity, rapid response and low cost which makes fluorescent detection a hopeful strategy for the recognition of metal ions [13,14]. Consequently, there has been an enhancing ambition for the synthesis of novel and low cost chemical sensors for Cu²⁺ towards the selective and accurate determination, which consist of rhodamine [15–18], coumarin [19–21], quinoline [22,23] pyrene [24,25] and other fluorophores [26–37]. In recent years, quinoline-based compounds are frequently used as fluorescence sensing system as the quinoline unit has large-conjugated molecular structure which shows excellent spectroscopic properties [38–40]. The nitrogen atom of the heterocyclic quinoline unit has the ability to act as

* Corresponding author.

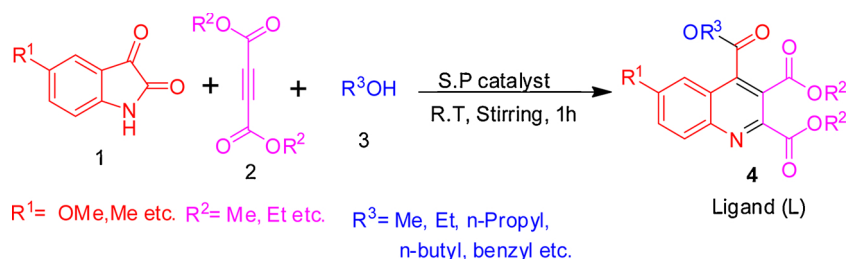
E-mail address: cmukhop@yahoo.co.in (C. Mukhopadhyay).

<https://doi.org/10.1016/j.jphotochem.2019.112211>

Received 31 August 2019; Received in revised form 29 October 2019; Accepted 2 November 2019

Available online 15 November 2019

1010-6030/ © 2019 Elsevier B.V. All rights reserved.



Scheme 1. Synthesis for the trisubstituted quinoline Ligands.

a site of a chelating towards metal ions [41–43]. Herein, we have synthesized fluorescent probes based upon quinoline moiety for the detection of Cu^{2+} with good selectivity in DMSO/ H_2O (2:8, v/v) mixed solvent using HEPES buffer solution (pH = 7.4).

Moreover, photo-physical studies on organic scaffolds containing electron donor (D) and also acceptor (A) group are continuously increasing the interest in fundamental research as they are broadly used as electro-optical switches, fluorescence probes and chemical sensing systems [44]. Generally in Intramolecular Charge Transfer (ICT) process, separation of charges takes place due to the charge transfer from a donor (D) part to an acceptor (A) site in a same molecule undergoing photo excitation. For this charge transfer, two different charges positive and negative localize in two different ends and separated by two functional groups in a same molecule and now this distribution of charge in the molecule enhances the molecular dipole moment [45]. As a result, electronic environments are rearranged in the same molecule. It is observed that compounds having both donor-acceptor groups undertake relaxation in the direction of a highly polar state and show evidence of irregular properties of dual emission in different solvents polar [46]. Due to the production of polar charge transfer (CT) stimulated state; the molecules show the anomalous behavior of emission which depends upon the polarity of the solvents. In this

paper we are reporting probes which contain strong “push-pull” electron system, with OMe / Me group as an electron donor and a carbonyl containing ester group as an electron acceptor. The probes have been successfully synthesized in superb yields and purity is high in just two simple steps. These probes can also be effectively applied to biological systems as they exhibited less cytotoxicity.

2. Results and discussion

Herein, we report that we have synthesized twelve substituted 6-methoxyquinoline-2, 3, 4-tricarboxylate fluorophores according to our previously reported methodology [47] (Scheme 1 and Table 1) and its fluorometric attempt toward effective detection of Cu^{2+} ions. The reported compounds are highly fluorescent due to the presence of strong “push-pull” electron system with OMe / Me groups acting as electron donor (D) and a carbonyl containing ester group (A) acting as electron acceptor, while the other compounds having H/Cl/Br/ NO_2 groups at 6-position of the compounds shows no fluorescence properties (Fig. 1).

This is because probably H/Cl/Br/ NO_2 groups are not able to provide sufficient electron density to the benzene ring of the quinoline derivatives, whereas OMe/Me groups probably do this.

Table 1
Synthesis of various 2, 3, 4-trisubstituted quinoline Ligands (L1-L12).

L1, 97% L1, 97%	L2, 95% L2, 95%	L3, 96% L3, 96%
L4, 89% L4, 89%	L5, 87% L5, 87%	L6, 85% L6, 85%
L7, 82% L7, 82%	L8, 81% L8, 81%	L9, 80% L9, 80%
L10, 76% L10, 76%	L11, 78% L11, 78%	L12, 90% L12, 90%

^[a]Reaction condition: Isatin (1; 1.00 mmol), diethylacetylenedicarboxylate (2, 1.00 mmol), ROH (3, 0.1 mL) and (MCM-41)-Pyridine catalyst (40 mg). S. P = (MCM-41)-Pyridine; ^[b] Isolated yield, R.T = Room Temp. L = Ligands.

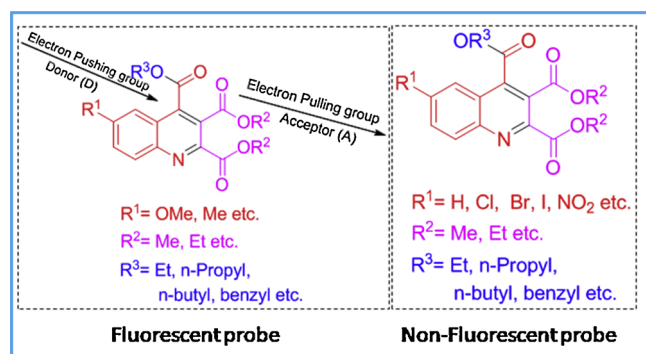


Fig. 1. Effect of donating and withdrawing groups on Fluorescent probe.

All the synthesized compounds were characterized by instrumental techniques, such as NMR (¹H/¹³C), IR, HRMS analysis, melting point measurements and CHN analysis (Electronic Supplementary information 2). We have also confirmed the final structure of the compound by the X-Ray single crystal analysis of the compound L1 and L4. Single crystal X-ray diffraction shows that compound L1 crystallizes in triclinic P-1 space group with Z = 2. The crystal structure of L1 (CCDC

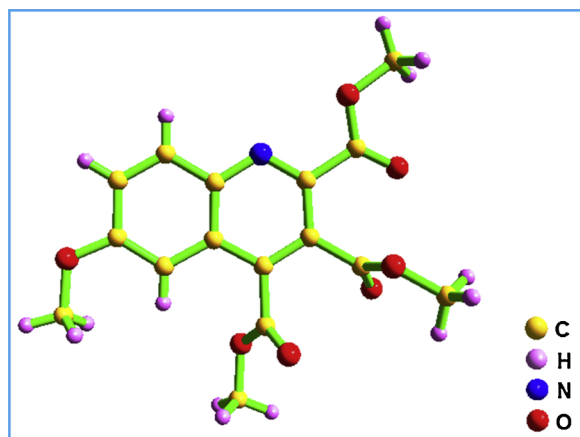


Fig. 2. Solid-state molecular structure of compound L1 (CCDC 1,914,745).

1,914,745) is shown in Fig. 2 and the relevant crystallographic data, selected bond lengths and bond angles are presented in Table S4 and Table S5 (Electronic Supplementary Information 1). The presence of π -systems in the compound L1, leads to strong intermolecular π ... π [within Cg(1)...Cg(2) = 3.615(9) Å {Cg(1) = N(3) - C(3) - C(4) - C(5) - C(30) - C(31), Cg(2) = C(6) - C(33) - C(32) - C(31) - C(30) - C(34)}] interactions between the closest neighbours (Fig. 3).

The compound L4 crystallizes in the monoclinic crystal system with space group P21/c with Z = 4 (Fig. 4) and the structure refinement parameters and crystallographic data of L4 (CCDC 1,903,253) is listed in Table S4 (Electronic Supplementary Information 1) and relevant bond lengths and angles are listed in Table S5 (Electronic Supplementary Information 1). The crystal structure of L4 shows the presence of strong intermolecular face-to-face π ... π stacking interactions between two aromatic rings with a centroid to centroid distance of 3.976 (8) Å [within Cg(2)...Cg(2) {Cg(2) = C(5) - C(6) - C(7) - C(8) - C(15) - C(50)}] (Fig. 5).

2.1. Photophysical study

2.1.1. Photophysical properties of compounds L3, L4, L7 and L9 when Cu²⁺ ion is present

The binding modes of synthesized chemosensors (L3, L4, L7 and L9) with Cu²⁺ were properly investigated with the help of UV-vis absorption spectroscopic analysis in DMSO/H₂O (2:8, v/v) using HEPES buffer solution (pH = 7.4). We noticed a significant changes in spectra while increasing concentrations of Cu²⁺ ions to the chemosensors (L3, L4, L7 and L9) as depicted in Figs. S 2–5 (Electronic Supplementary Information 1). The emission spectrum of the fluorescent chemosensors (L3, L4, L7 and L9) (5×10^{-6} M) were recorded in DMSO/H₂O (2:8, v/v) HEPES buffer solution (pH = 7.4). The free chemosensors (L3, L4, L7 and L9) (λ_{ex} = 350.32 nm, 350.14 nm, 352.01 nm and 351.25 nm; λ_{em} = 459.56 nm, 462.39 nm, 465.58 nm and 457.54 nm) displayed strong emission intensity with quantum yield (ϕ) of 0.512 (L3), 0.196 (L4), 0.267 (L7) and 0.325 (L9) respectively.

The emission intensity of chemosensors (L3, L4, L7 and L9) significantly decreases when various concentrations of Cu²⁺ (0–10 μ M) were added to these solutions [(Fig. 6), (Fig. 7) and {Figure S6 and S7 (Electronic Supplementary Information 1)}] and the fluorescence quantum yields (ϕ) are reduced to 0.055 (L3 + Cu²⁺), 0.061 (L4 + Cu²⁺), 0.057 (L7 + Cu²⁺) and 0.029 (L9 + Cu²⁺) respectively (Table

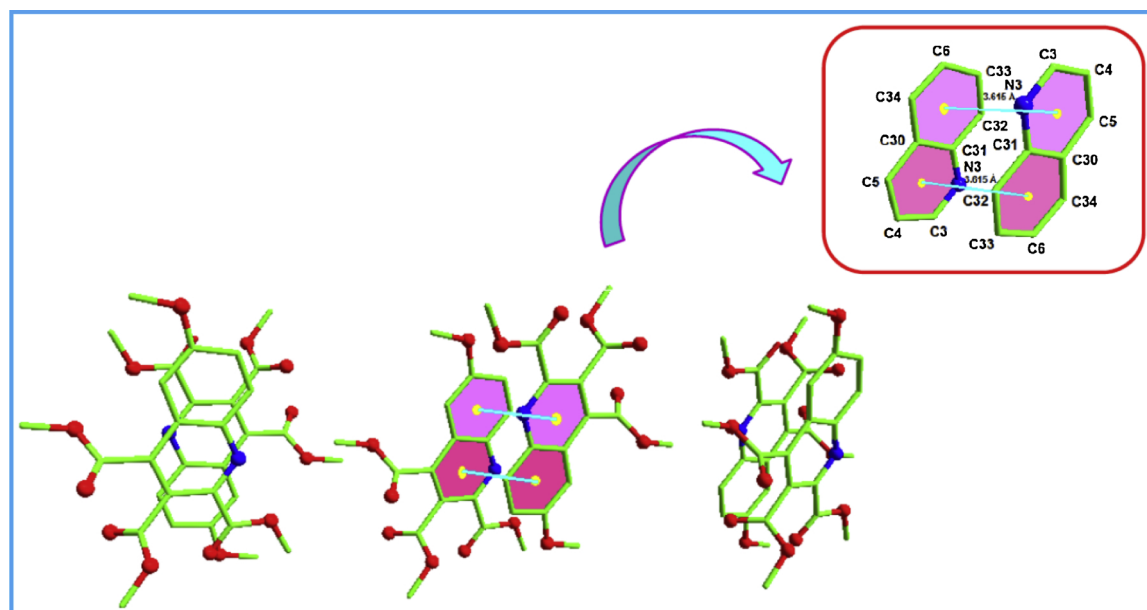


Fig. 3. The inter-molecular π - π interactions in the crystal packing of compound L1 (Hydrogen atoms are omitted for clarity).

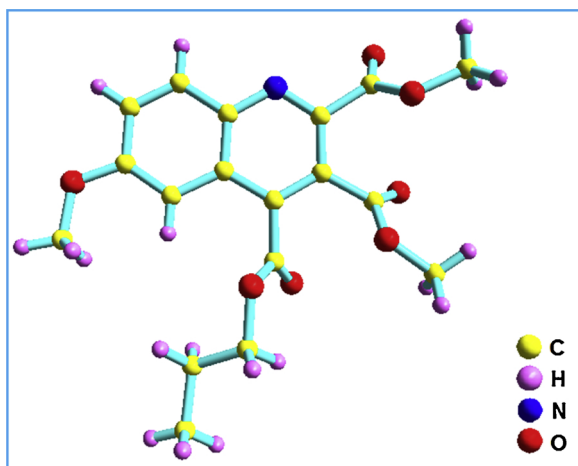


Fig. 4. Solid-state molecular structure of compound L4 (CCDC 1,903,253).

S3, Electronic Supplementary Information 1). To appraise the selectivity and sensitivity of the chemosensors (L3, L4, L7 and L9) for Cu^{2+} ion, competitive experiment was designed while other various metal ions such as Na^+ , Li^+ , K^+ , Mg^{2+} , Ca^{2+} , Mn^{2+} , Ni^{2+} , Ba^{2+} , Co^{2+} , Fe^{2+} , Cd^{2+} , Zn^{2+} , Hg^{2+} , Sr^{2+} , Pb^{2+} and Al^{3+} present in a mix solution of DMSO and H_2O (DMSO: H_2O :: 2:8, v/v) HEPES buffer solution (pH = 7.4).

It was observed that the chemosensors (L3, L4, L7 and L9) could efficiently sense Cu^{2+} ion when other common metal ions are present. These results suggested that selective binding of chemosensors (L3, L4, L7 and L9) with Cu^{2+} will remain constant in presence of other ions [(Fig. 8), (Fig. 9) and {Figure S8 and S9 (Electronic Supplementary Information 1)}]. We have also studied the absorption and emission spectral output of the chemosensors (L3, L4, L7 and L9) in various solvents (Table S2, Electronic Supplementary Information 1). The Job's plot indicated 1:1 stoichiometric ratio between the chemosensors (L3, L4, L7 and L9) and Cu^{2+} (Figure S10-S13, Electronic Supplementary Information 1). The positive ion mass spectrum for the reaction of chemosensor L3 with Cu^{2+} supports the above facts (Figure

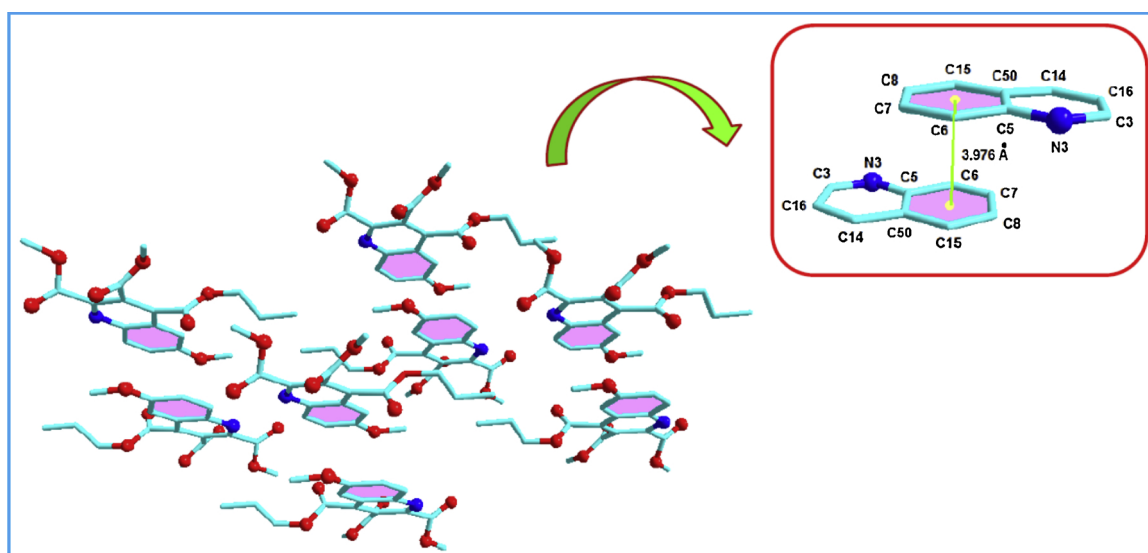


Fig. 5. The inter-molecular π - π interactions in the crystal packing of compound L4 (Hydrogen atoms are omitted for clarity).

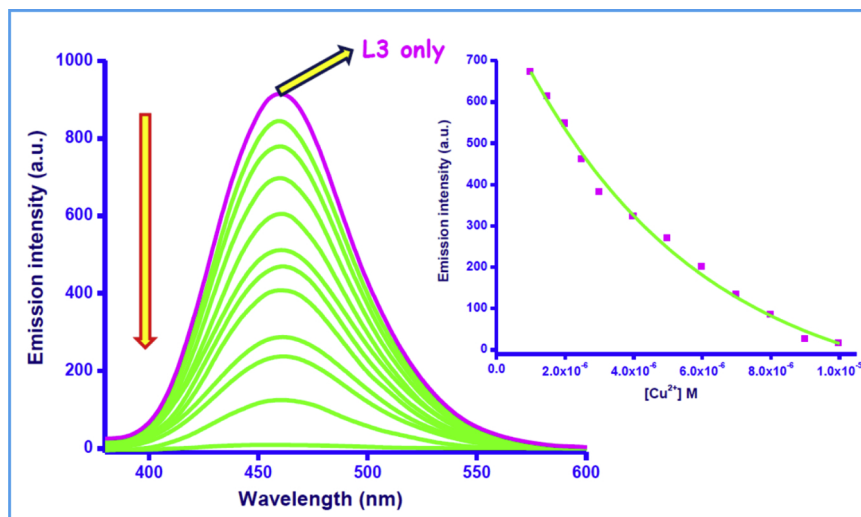


Fig. 6. Emission spectra of L3 [5×10^{-6} (M)] in the presence of increasing amounts of $[\text{Cu}^{2+}]$ (0, 0.5, 1, 2, 3, 4, 5, 6, 7, 8, 9 and 10 ($\times 10^{-6}$) (M) in DMSO/ H_2O (2:8, v/v) HEPES buffer (pH = 7.4) solution. (λ_{exc} = 350.32 nm, λ_{em} = 459.56 nm). Inset: Emission intensity of Fluorescent probe L3 at 459.56 nm as function of $[\text{Cu}^{2+}]$.

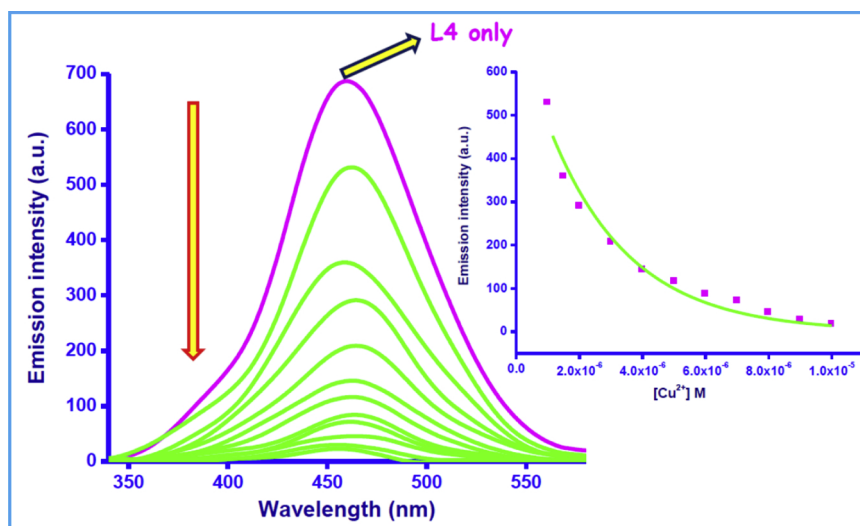


Fig. 7. Emission spectra of L4 (5×10^{-6} M) in the presence of increasing amounts of $[\text{Cu}^{2+}]$ (0, 0.5, 1, 2, 3, 4, 5, 6, 7, 8, 9 and 10 ($\times 10^{-6}$ M) in DMSO/ H_2O (2:8, v/v) HEPES buffer (pH = 7.4) solution ($\lambda_{\text{ex}} = 350.14$ nm, $\lambda_{\text{em}} = 462.39$ nm). Inset: Fluorescence emission intensity of L4 at 462.39 nm as a function of $[\text{Cu}^{2+}]$.

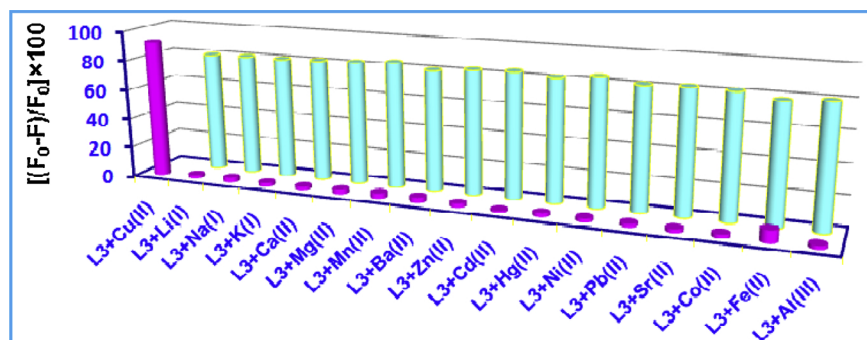


Fig. 8. Fluorescence emission spectra of L3 (5×10^{-6} M) in the presence of 4 equiv. of different cations (Li^+ , Na^+ , K^+ , Ca^{2+} , Mg^{2+} , Mn^{2+} , Ba^{2+} , Zn^{2+} , Cd^{2+} , Hg^{2+} , Ni^{2+} , Pb^{2+} , Sr^{2+} , Co^{2+} , Fe^{2+} and Al^{3+}) except 2 equiv. of Cu^{2+} in solution [the magenta bar portion ($\text{L3} + \text{Cu}^{2+}$, $\text{L3} + \text{Li}^+$, $\text{L3} + \text{Na}^+$, $\text{L3} + \text{K}^+$, $\text{L3} + \text{Ca}^{2+}$, $\text{L3} + \text{Mg}^{2+}$, $\text{L3} + \text{Mn}^{2+}$, $\text{L3} + \text{Ba}^{2+}$, $\text{L3} + \text{Zn}^{2+}$, $\text{L3} + \text{Cd}^{2+}$, $\text{L3} + \text{Hg}^{2+}$, $\text{L3} + \text{Ni}^{2+}$, $\text{L3} + \text{Pb}^{2+}$, $\text{L3} + \text{Sr}^{2+}$, $\text{L3} + \text{Co}^{2+}$, $\text{L3} + \text{Fe}^{2+}$ and $\text{L3} + \text{Al}^{3+}$)]. Fluorescence intensity of a mixture of L3 (5×10^{-6} M) with other metal ions (20×10^{-6} M) followed by addition of Cu^{2+} (10×10^{-6} M) to the DMSO/ H_2O (2:8, v/v) HEPES buffer (pH = 7.4) solution [the cyan bar portion ($\text{L3} + \text{Li}^+ + \text{Cu}^{2+}$, $\text{L3} + \text{Na}^+ + \text{Cu}^{2+}$, $\text{L3} + \text{K}^+ + \text{Cu}^{2+}$, $\text{L3} + \text{Ca}^{2+} + \text{Cu}^{2+}$, $\text{L3} + \text{Mg}^{2+} + \text{Cu}^{2+}$, $\text{L3} + \text{Mn}^{2+} + \text{Cu}^{2+}$, $\text{L3} + \text{Ba}^{2+} + \text{Cu}^{2+}$, $\text{L3} + \text{Zn}^{2+} + \text{Cu}^{2+}$, $\text{L3} + \text{Cd}^{2+} + \text{Cu}^{2+}$, $\text{L3} + \text{Hg}^{2+} + \text{Cu}^{2+}$, $\text{L3} + \text{Ni}^{2+} + \text{Cu}^{2+}$, $\text{L3} + \text{Pb}^{2+} + \text{Cu}^{2+}$, $\text{L3} + \text{Sr}^{2+} + \text{Cu}^{2+}$, $\text{L3} + \text{Co}^{2+} + \text{Cu}^{2+}$, $\text{L3} + \text{Fe}^{2+} + \text{Cu}^{2+}$ and $\text{L3} + \text{Al}^{3+} + \text{Cu}^{2+}$)] ($\lambda_{\text{ex}} = 350.32$ nm, $\lambda_{\text{em}} = 459.56$ nm).

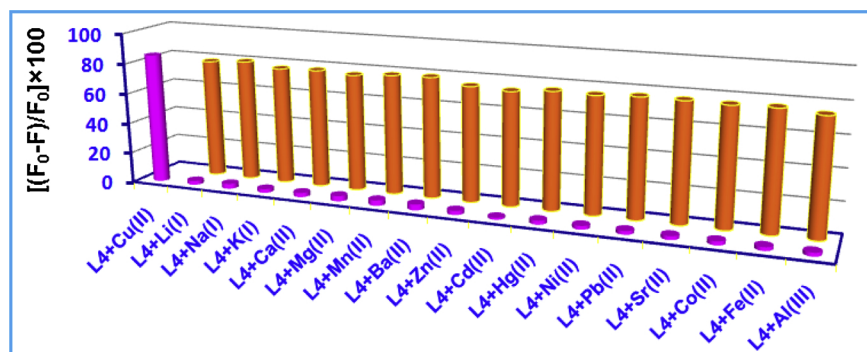
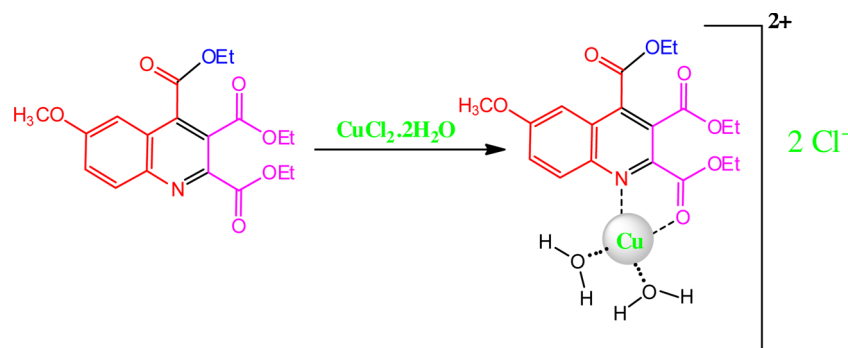


Fig. 9. Fluorescence emission spectra of L4 (5×10^{-6} M) in the presence of 4 equiv. of different cations (Li^+ , Na^+ , K^+ , Ca^{2+} , Mg^{2+} , Mn^{2+} , Ba^{2+} , Zn^{2+} , Cd^{2+} , Hg^{2+} , Ni^{2+} , Pb^{2+} , Sr^{2+} , Co^{2+} , Fe^{2+} and Al^{3+}) except 2 equiv. of Cu^{2+} in solution [the magenta bar portion ($\text{L4} + \text{Cu}^{2+}$, $\text{L4} + \text{Li}^+$, $\text{L4} + \text{Na}^+$, $\text{L4} + \text{K}^+$, $\text{L4} + \text{Ca}^{2+}$, $\text{L4} + \text{Mg}^{2+}$, $\text{L4} + \text{Mn}^{2+}$, $\text{L4} + \text{Ba}^{2+}$, $\text{L4} + \text{Zn}^{2+}$, $\text{L4} + \text{Cd}^{2+}$, $\text{L4} + \text{Hg}^{2+}$, $\text{L4} + \text{Ni}^{2+}$, $\text{L4} + \text{Pb}^{2+}$, $\text{L4} + \text{Sr}^{2+}$, $\text{L4} + \text{Co}^{2+}$, $\text{L4} + \text{Fe}^{2+}$ and $\text{L4} + \text{Al}^{3+}$)]. Fluorescence intensity of a mixture of L4 (5×10^{-6} M) with other metal ions (20×10^{-6} M) followed by addition of Cu^{2+} (10×10^{-6} M) to the DMSO/ H_2O (2:8, v/v) HEPES buffer (pH = 7.4) solution [the red bar portion ($\text{L4} + \text{Li}^+ + \text{Cu}^{2+}$, $\text{L4} + \text{Na}^+ + \text{Cu}^{2+}$, $\text{L4} + \text{K}^+ + \text{Cu}^{2+}$, $\text{L4} + \text{Ca}^{2+} + \text{Cu}^{2+}$, $\text{L4} + \text{Mg}^{2+} + \text{Cu}^{2+}$, $\text{L4} + \text{Mn}^{2+} + \text{Cu}^{2+}$, $\text{L4} + \text{Ba}^{2+} + \text{Cu}^{2+}$, $\text{L4} + \text{Zn}^{2+} + \text{Cu}^{2+}$, $\text{L4} + \text{Cd}^{2+} + \text{Cu}^{2+}$, $\text{L4} + \text{Hg}^{2+} + \text{Cu}^{2+}$, $\text{L4} + \text{Ni}^{2+} + \text{Cu}^{2+}$, $\text{L4} + \text{Pb}^{2+} + \text{Cu}^{2+}$, $\text{L4} + \text{Sr}^{2+} + \text{Cu}^{2+}$, $\text{L4} + \text{Co}^{2+} + \text{Cu}^{2+}$, $\text{L4} + \text{Fe}^{2+} + \text{Cu}^{2+}$ and $\text{L4} + \text{Al}^{3+} + \text{Cu}^{2+}$)] ($\lambda_{\text{ex}} = 350.14$ nm, $\lambda_{\text{em}} = 462.39$ nm).

S1, Electronic Supplementary Information 1). The stability constant (K) for the chemosensors (L3, L4, L7 and L9)– Cu^{2+} complex were investigated from the Benesi–Hildebrand plots (Figure S14–17, Electronic Supplementary Information 1). The calculated stability constants values for L3, L4, L7 and L9 are (31.22×10^4), (31.36×10^4), (33.51×10^4) and (32.57×10^4) respectively. From the fluorescence

titration experiments, LOD values (the detection limit) of the representative chemosensors (L3, L4, L7 and L9) were determined (Figure S18–21 and Table S3, Electronic Supplementary Information 1). The calculated LOD values for L3, L4, L7 and L9 are (3.01×10^{-7}), (4.82×10^{-7}), (5.17×10^{-7}) and (6.23×10^{-7}) respectively. We have also determined the LOQ (Limit of Quantification) and the values



Scheme 2. Probable binding mode of synthesised chemosensors L3 with Cu^{2+} .

are (10.03×10^{-7}) , (16.07×10^{-7}) , (17.23×10^{-7}) , (20.76×10^{-7}) for L3, L4, L7 and L9 respectively (Table S3, Electronic Supplementary Information 1). The linear concentration ranges for L3, L4, L7 and L9 are $(1.0 \times 10^{-6} - 10.0 \times 10^{-6})$, $(3.0 \times 10^{-6} - 9.0 \times 10^{-6})$, $(1.0 \times 10^{-6} - 10.0 \times 10^{-6})$ and $(1.0 \times 10^{-6} - 9.0 \times 10^{-6})$ respectively. From the all above experimental observations, it can be said that ligand L3 is suitable as compared to the other sensors. That's why we are basically focused on ligand L3.

A probable binding mode of chemosensors L3 with Cu^{2+} ion is shown in Scheme 2. Here, we propose that the O-atom of ester group and N-atom of quinoline ring take part in the complexation with Cu^{2+} ions. The four co-ordination of copper is satisfied by one O atom, one N atom and two molecules of water. Actually the charge of the whole complex is positive (2+) and the chloride ions are in the solution to maintain charge balance. ESI-MS mass spectra (Figure S1, Electronic Supplementary Information 1), DFT structure optimisation and Job's plot are the evidences in support of our proposed complexation mechanism (Scheme 2).

The sensitivity and selectivity of our proposed route has been compared with the prior literatures for the recognition of Cu^{2+} ions (Table 2). We believe that this chemosensor is found to be better than or comparable with the sensitivity of previously reported sensors in terms of both LOD value as well as binding constant value.

Moreover, the procedure of our synthesised probe has superiority over the other existing methods (Table 2) because our methodology involves (a) simple starting materials (b) short reaction time (c) room temperature (25-30°C), no heat or reflux needed (d) high to excellent yields (e) easy to separate the product etc.

As the reversibility of the chemosensor represents a significant parameter, we carefully investigated the reversibility of the sensors by means of alternate addition of $\text{Na}_2\text{H}_2\text{EDTA}$ and Cu^{2+} (Figure S22-25, Electronic Supplementary Information 1). The repeatability of the response was also evaluated by performing the above experiment every

two minutes by twenty consecutive cycles and the Fig. 10, Fig. 11 and (Figure S26-27, Electronic Supplementary Information 1) depict well defined behavior suggesting repeatability of the probes.

The fluorescence responses of chemosensors (L3, L4, L7 and L9) in presence and also in absence of Cu^{2+} were also explored in DMSO/ H_2O solution [(2:8, v/v)] when the pH was adjusted with the help of HCl and NaOH (Figure S 28, Electronic Supplementary Information 1). In the pH region 6.0–9.0, free chemosensors (L3, L4, L7 and L9) retained their fluorescent nature and the fluorescence intensity of chemosensors (L3, L4, L7 and L9)- Cu^{2+} complexes kept almost constant for wide range of pH 3.0–11.0 in the solution. Thus, the chemosensors (L3, L4, L7 and L9) can be effectively used as probe under biological conditions at pH = 7.4. Fluorescence life time measurements of chemosensors (L3,

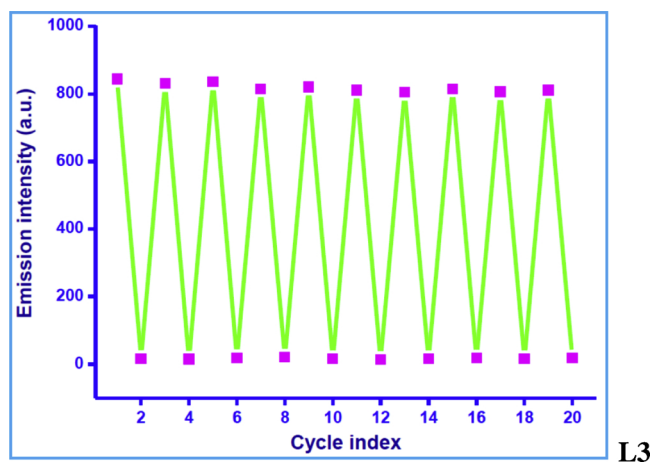


Fig. 10. Reversible changes in emission intensity of L3 (5×10^{-6} M) at 459.56 nm after the sequential addition of Cu^{2+} and EDTA.

Table 2

. Comparison of the synthesised probe with other sensing probes for detection of Cu^{2+} ion.

Sr. No.	Chemosensors	Detection Type	Limit of Detection (M)	Binding Constants (M^{-1})	Applications	References
1	Quinoline and pyridine fluorophores	On-Off	6.17×10^{-7}	3.179×10^5	Cell imaging	[48]
2	Spiro[indoline-3,4'-pyridine]	On-Off	5.51×10^{-7}	3.340×10^5	Cell imaging	[49]
3	Coumarin based	On-Off	-a	0.26×10^5	-a	[50]
4	Hydroxyindole fused isocoumarin	On-Off	70.7×10^{-7}	-a	-a	[51]
5	Coumarin and quinoline moiety	On-Off	25.0×10^{-7}	0.0365×10^5	Living cell imaging	[52]
6	Calix [4] arene derivatives	On-Off	10.5×10^{-7}	-a	-a	[53]
7	Rhodamine derivatives	Off-On	2.8×10^{-7}	0.118×10^5	Bio-imaging of live HeLa cells	[54]
8	Curcumin derivatives	Off-On	25.4×10^{-7}	-a	Bio-imaging	[55]
9	Rhodamine derivatives	Off-On	6.96×10^{-7}	15.2×10^6	Bio-imaging	[56]
10	3-(1H-benzimidazol-2-yl)-2-hydroxy-benzoate sodium	On-Off	27.7×10^{-7}	3.22×10^5	Living cell imaging	[57]
11	BINOL- based fluorescent sensor	On-Off	40.0×10^{-7}	0.003×10^5	-a	[58]
12	Tryptophan-dansyl chloride	On-Off	5.0×10^{-7}	-a	-a	[59]
13	Quinoline based	On-Off	3.01×10^{-7}	3.122×10^5	HEK 293 cell imaging	This work

^aNot provided.

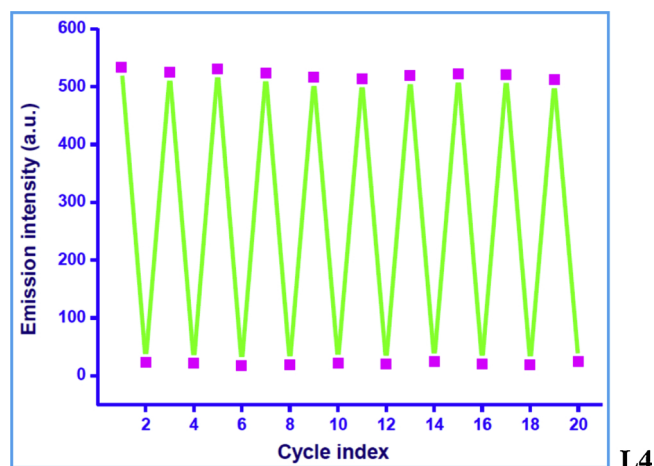


Fig. 11. Reversible changes in emission intensity of L4 (5×10^{-6} M) at 462.39 nm after the sequential addition of Cu^{2+} and EDTA.

L4, L7 and L9) and its Cu^{2+} complexes were measured by applying the TCSPC (time-correlated single photon counting) technique (Figure S29, Electronic Supplementary Information 1) and the results were put into a Table S1 (Electronic Supplementary Information 1). The radiative and non-radiative decay constants were calculated for chemosensors (L3, L4, L7 and L9) and Cu^{2+} : probe entity.

A hopeful analytical test of L3 for detection of Cu^{2+} was performed based upon paper-based fluorescent sensing system (Fig. 12). It was noted that L3 gave no emission in daylight in absence or presence of Cu^{2+} . But it displays almost light sky emission (under UV light) in absence of Cu^{2+} and changes its colour to colourless dark after the addition of Cu^{2+} solution (under UV light). Hence, the probe L3 exhibited a turn-off fluorescence response toward Cu^{2+} with selectivity, reversibility, repeatability, excellent stability, rapidity and operational expediency and all these features offer robustness to the probes.

Furthermore, to investigate the sensing applicability of the system L3 in real samples, we estimated the concentrations of Cu^{2+} in water samples in the form of laboratory distilled water, tap water and river

water (Ganges) without further processing. We found the satisfactory recoveries in a range of 98%–102.4% for Cu^{2+} (Table 3). The relative errors and the accuracies in the three real water samples were found in the range of 1.2%–2.4% and around 98% for Cu^{2+} which offers good agreement between the added and measured values of the spiked samples. From these analytical results, it can be concluded that probe L3 is suitable for determination of Cu^{2+} in real water samples with high precision and good accuracy leading to a sustainable method in the domain of public health.

2.2. DFT calculation

The ground state geometry of the complex between representative compound L1 and Cu^{2+} metal was optimized with DFT/B3LYP/6-31G* basis set. It was seen from experiment that Cu^{2+} form complex in 1:1 stoichiometric ratio, accordingly Quantum chemical structure was optimized (Fig. 13).

Fig. 13 indicates that Cu^{2+} was precisely centered over the O-atom with a distance of 2.06 Å between metal and ligand. A TDDFT excitation calculation using DFT/B3LYP/6-31G* in DMSO solvent medium using IEFPCM model of solvation were carried out for both free and metal complexed ion to judge the absorption phenomena and FMO features. The role of FMOs in the degree of interaction was utilized for the interactions of metal ion and the ground state energy parameters have also been represented in Table 4 and in Fig. 14.

On interaction with metal ion, band gap of compound (4.39 eV) was moved to low energy (2.66 eV) i.e. to longer wavelength. Both the HOMO-LUMO energies of free compound were stabilized upon formation of complex with metal ion. The FMO features of Table 4 and Fig. 14 indicates that in free compound, both HOMO and LUMO are distributed over the quinoline unit including the N- and O-donor centers. On metal complex SOMO and (HOMO – 1) is almost remaining the same as that of free compound but LUMO was centered over the Cu^{2+} centre (Fig. 14), thus indicating a clear LMCT transition.

In formation of metal complex both C–N and CO– bond length suffers changes as shown in Fig. 13 and Table 4. 1.20 Å C=O is elongated to 1.33 Å which clearly indicates double bonded O-centre donated electron to metal centre much and has almost lost its unstauration. TDDFT calculation shows similar result of large bathochromic

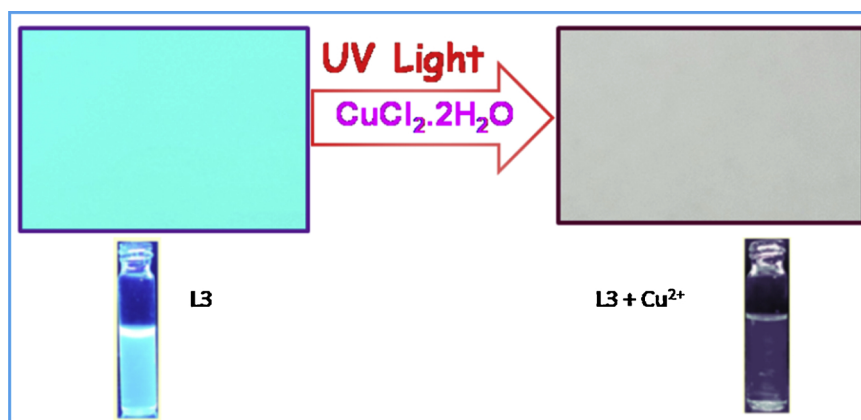


Fig. 12. Photographic image of L3 on paper strip in the absence and presence of Cu^{2+} under UV light (365 nm).

Table 3

Analytical results for the determination of Cu^{2+} in real water samples.

	Type of water Samples	Cu^{2+} Added (M)	Cu^{2+} Detected (M)	Recovery (%)	Relative error (%)
Cu^{2+}	Laboratory distilled water	5×10^{-6}	5.12×10^{-6}	102.4	2.4
	Tap water	5×10^{-6}	4.89×10^{-6}	98	2.2
	Ganges River water	5×10^{-6}	5.06×10^{-6}	101.2	1.2

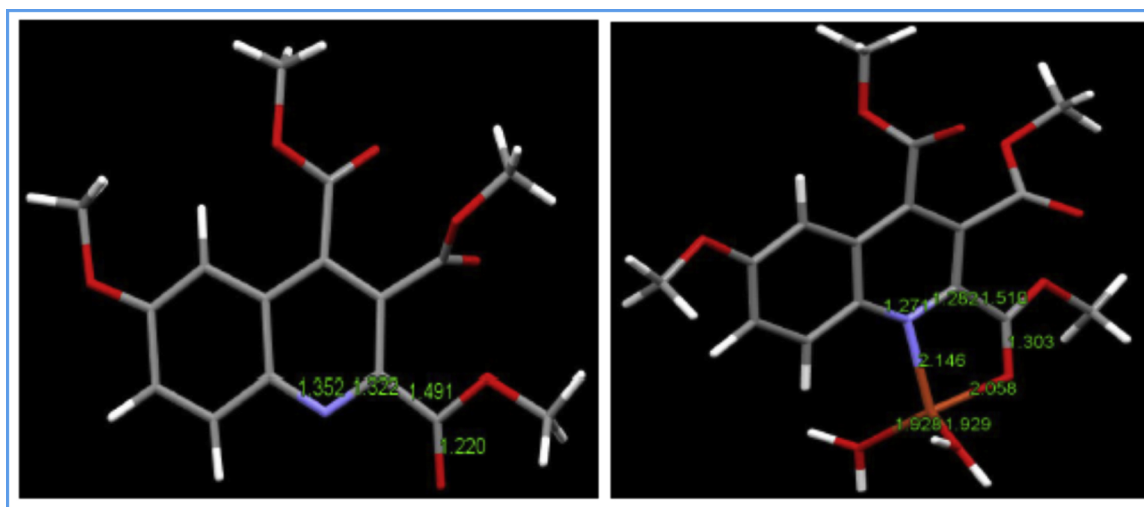


Fig. 13. DFT optimized ground state geometry of L1 and its Cu²⁺ complex.

Table 4

Calculation of HOMO-LUMO energies band gap and bond length of L1 and L1-Cu²⁺ complex.

Species	$\epsilon_{\text{HOMO or SOMO}}$ (eV)	ϵ_{LUMO} (eV)	Band gap (eV)	Bond length (Å)			
				C-N	C-O	N-Cu ²⁺	O-Cu ²⁺
Free L1	-6.6490	-2.2565	4.39	1.35	1.22	-	-
L1/Cu ²⁺ -complex	-12.6110	-9.9485	2.66	1.32	1.30	2.15	2.06
				1.27	1.28		
				1.28			

shift on LMCT as that obtained experimentally. This calculation gives accurate result with reasonable minimization of oscillators strength associated with UV-vis absorption in case of Cu ion complex ($f = 0.0072$) compared to free L1 ($f = 0.2143$). This minimization of oscillator's strength clearly indicates cause of lowering of absorbance on interacting with Cu²⁺. This also reflects simultaneous fluorescence quenching effect alongside of non-radiative decay due to paramagnetic

realm of Cu (II)-fluorophore complexation as explained by Yang et. al. [60]. The first excitation parameters (**Electronic supplementary Information 3**) of Cu²⁺ complex of L1, clearly exhibited that there is no SOMO-LUMO transition (deactivation of which might be spin forbidden), rather it is mostly contributed by HOMO-1 to LUMO and HOMO-4 to SOMO. So there is clear chance of mixing in radiative decay with non-radiative one as predicted by Yang et. al.

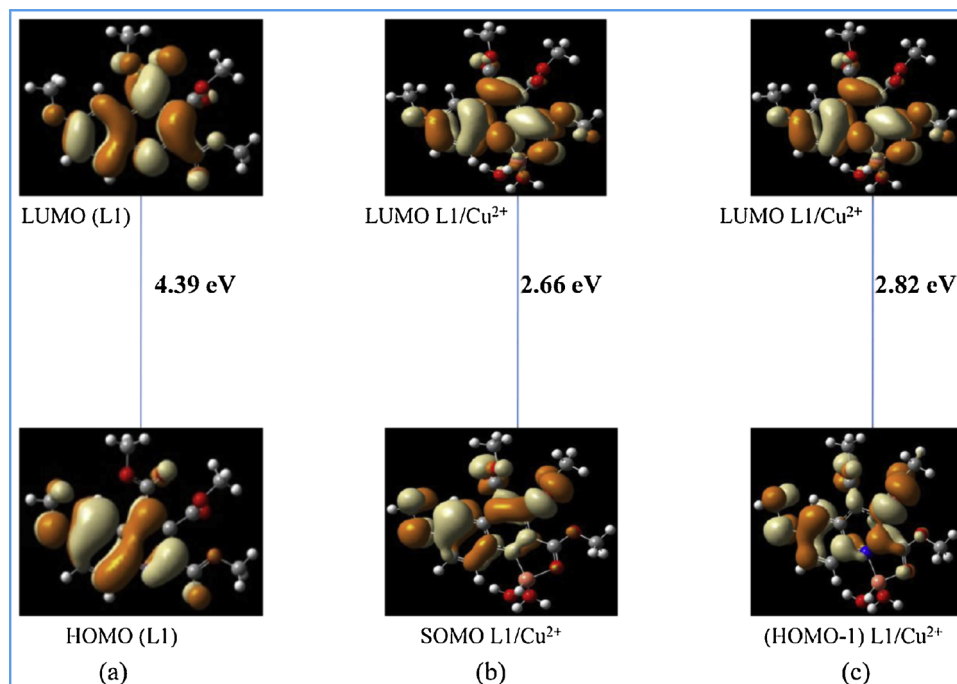


Fig. 14. Energy profile diagram of free L1 and its Cu²⁺ complex.

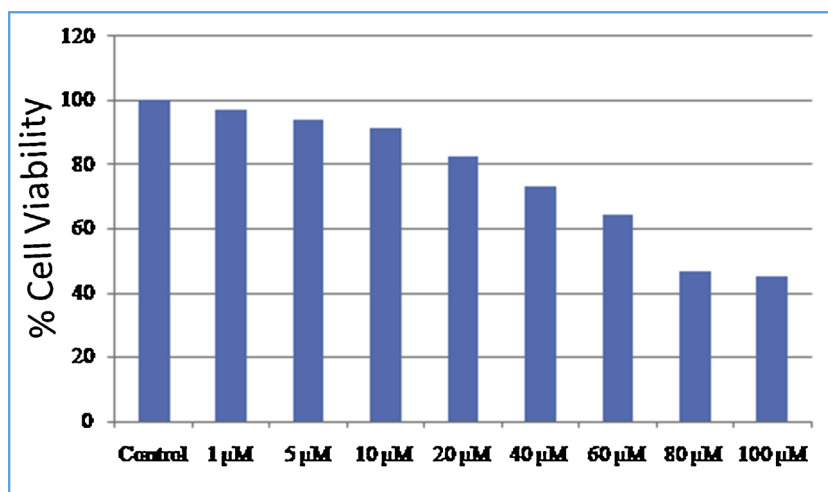


Fig. 15. Percent (%) cell viability of HEK 293 cells when treated with various concentrations (1 – 100 μM) of L3 for 24 h determined by MTT assay.

3. Biological application

3.1. Result

In order to consider the strong selective binding affinity of L3 with Cu^{2+} ions, it has been further verified for its Cu^{2+} detection ability in the living cell line. It was noticed that cell viability was around 90% for L3 at $10\mu\text{M}$, after that the cell viability of the HEK 293 cells reduced. That is why, we have carried out further experiments with $10\mu\text{M}$ of L3 for further treatment. The ligand L3 showed presence of prominent intracellular fluorescence in HEK 293 cells when treated with $10\mu\text{M}$ of the sample and was incubated for 30 min (Fig. 15); the intracellular fluorescence was found to be prominently. $10\mu\text{M}$ of Cu^{2+} was used to incubate HEK 293 cells for 60 just minutes at 37°C , followed by the incubation with $10\mu\text{M}$ of L3 for 30 min at 37°C .

Keeping the ligand L3 concentration stable ($10\mu\text{M}$) and growing the

concentration of Cu^{2+} (from $10\mu\text{M}$ to $20\mu\text{M}$ and finally $40\mu\text{M}$) results Cu^{2+} ion concentration-dependent reduction in emission of intracellular blue fluorescence originated by complex formation with L3 (Fig. 16). Intense quenching of intracellular fluorescence was observed due to formation of complex between Cu^{2+} and the probe L3 nearly when $40\mu\text{M}$ of Cu^{2+} was used.

Therefore, this ligand with low cytotoxic value and biocompatible for intracellular Cu^{2+} ion detection can be utilized to detect Cu^{2+} in biological samples.

4. Experimental

4.1. General information of materials and instruments

All marketable chemicals were bought from Aldrich, Spectrochem or USA, India and all of them were used with making no further

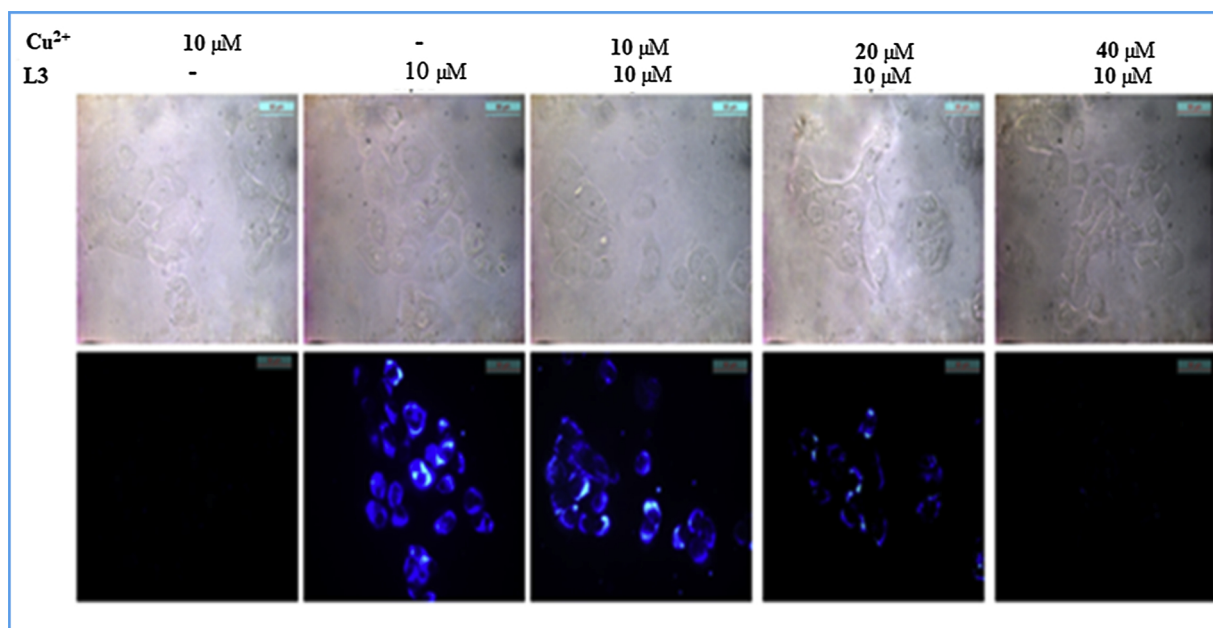


Fig. 16. The fluorescence imaging of HEK 293 cells were captured at 40X magnification after incubation with $10\mu\text{M}$, $20\mu\text{M}$ and finally $40\mu\text{M}$ of Cu^{2+} for just 60 min at 37°C , then washed thrice with 1X PBS, and incubation with $10\mu\text{M}$ of L3 at 37°C for 60 min. The upper panel represents the bright field images showing the morphological features of the cells after incubation with Cu^{2+} and/or L3; the lower panel represents the fluorescence emission *in vivo* after incubation with Cu^{2+} and/or L3. The images show bright fluorescence signal by the fluorophore L3 ($10\mu\text{M}$) when Cu^{2+} ion is absent, while the fluorescence slowly decreases with use of higher concentration of Cu^{2+} ions.

purification. All the solvents were utilized as we received. All reactions were carried in a round-bottomed flask with a magnetic stir bar at room temperature (25–30°C) with taking no precautions to exclude moisture and air. The improvement of the reaction was checked with the help of a glass sheets pre-coated TLC with binder silica gel with 300 mesh size (Spectrochem) and column chromatography was done using 100–200 mesh silica gel. $^1\text{H}/^{13}\text{C}$ NMR spectra of all the compounds were recorded in a 300 MHz NMR instrument (Bruker) using CDCl_3 as solvent with TMS as reference. HRMS-ESI sources were obtained by a Waters XEVO-G2S Q TOF mass spectrometer. For elemental analyses 2400 Series II CHNS Analyzer, Perkin Elmer USA was used. Furthermore, we have recorded melting points with the help of an open capillary on a melting point (electrical) apparatus. Using KBr pellets, IR experiment was carried out on Perkin Elmer RX-1 FTIR spectrophotometer. The single crystal structure of the compound was confirmed by an X-ray crystallographic analysis in a Bruker SMART diffractometer instrument.

4.2. Synthesis

At first, a mixture of 5-methoxy (or methyl) isatin (1 mmol) and acetylenedicarboxylates (1 mmol) in presence of (MCM-41)-Pyridine (40 mg) were taken in alcohol (0.1 mL) and continuously stirred for 1 h at room temperature (25–30°C). The progression of the reaction checked by thin layer chromatography (TLC) using aluminium plate which is coated with silica gel (Merck). When the reaction was completed, the reaction solution was diluted with DCM, filtered and washed several times with DCM so that the product separates as filtrate from the solid catalyst (residue). The residual catalyst part was then washed with water, DCM, methanol dried in oven and used for next cycles. The solvent (main filtrate part) was removed by rotary evaporator instrument. Finally, column chromatography was performed with the crude to afford the expected product (solid) using 6–8 % EtOAc in petroleum ether (60–80 °C) as eluant. Also we have purified some synthesised compounds by preparative TLC as it enhances the green impact of our methodology. All the obtained products were characterized by $^1\text{H}/^{13}\text{C}$ NMR, IR, CHN analysis, melting point measurements. HRMS of few compounds has been provided.

4.3. Single-crystal X-ray crystallography

Single-crystal X-ray diffraction data of chemosensor (L1 and L4) were performed on Nonius APEX-II diffractometer with CCD-area detector at 296 K using graphite-monochromated Mo-K α radiation ($\lambda = 0.71073$ Å). The program SMART [61] was used for collecting frames of data, indexing reflections, and determining lattice parameters, SAINT was used for integration of the intensity of reflections and scaling, SADABS [62] for absorption correction, and SHELXTL [63,64] for space group, structure determination and least-squares refinements on F^2 . The structures were solved by direct methods and refined by full-matrix least squares calculations using SHELXTL software [65] All non-hydrogen atoms were refined in the anisotropic approximation against F^2 of all reflections. The hydrogen atoms attached to carbon atoms were placed in calculated positions and refined isotropically riding on their parent atoms. The crystallographic data and some features of the structure refinements are summarized in Table S4 (Electronic Supplementary Information 1). Crystallographic details are available in CIF format. CCDC numbers 1,914,745 (for L1) and 1,903,253 (for L4). These data can be obtained free of charge from the Cambridge Crystallographic Data Centre via www.ccdc.cam.ac.uk/data_request/cif.

4.4. Photophysical Study

4.4.1. General Information

We recorded the ESI-MS on a Qtof Micro YA263 mass spectrometer. The emission and absorption spectra were also recorded on

Perkin-Elmer LS55 fluorimeter and Hitachi UV-Vis U-3501 spectrophotometer respectively.

4.4.2. Fluorescence quantum yield calculation in solution

Fluorescence quantum yield was calculated by using quinine sulphate ($\phi_R = 0.546$ in 0.1 M H_2SO_4) as standard. The quantum yield was determined based on the following formula.

$$\phi_s = \phi_R \frac{A_s}{A_R} \times \frac{Abs_R}{Abs_S} \times \frac{\eta_s^2}{\eta_R^2}$$

Where A terms signify the integrated area which is under the fluorescence curve, Abs indicates absorbance, η is the refractive index of the medium and the term ϕ denotes fluorescence quantum yield. Subscripts R and S denote the parameters for reference and the studied sample respectively.

4.4.3. Preparation of Sample for UV-vis and fluorescence spectral experiments

For UV-vis and emission titration studies, a stock solution of compounds (L3, L4, L7 and L9) were prepared by using of DMSO/ H_2O mix solvent (2:8, v/v) HEPES buffer solution (pH = 7.4). We also prepared solutions of various metal ions in DMSO/ H_2O (2:8, v/v) medium. For the titration of UV-vis experiment, a stock solution of these compounds (L3, L4, L7 and L9) 10^{-3} (M) were filled up separately in a quartz optical cell having optical path length of 1.0 cm to attain a ultimate concentration of solution of the compounds 5×10^{-6} (M) in 2000 μL . Then using a micropipette, we added metal ions to the solution of these compounds. For emission titrations, we took 10^{-3} (M) solution of each compound (L3, L4, L7 and L9) 10 μL in a 1.0 cm path length quartz optical cell of in 2000 μL and then by using micropipette, stock solutions of metal ions were gradually added to it. Spectral datas were taken at 1 min after the metal ions addition for both titrations. For this titration experiment, we used the cations, viz. $[\text{Na}^+, \text{Li}^+, \text{K}^+, \text{Mg}^{2+}, \text{Ca}^{2+}, \text{Mn}^{2+}, \text{Cu}^{2+}, \text{Ba}^{2+}, \text{Co}^{2+}, \text{Ni}^{2+}, \text{Fe}^{2+}, \text{Zn}^{2+}, \text{Cd}^{2+}, \text{Pb}^{2+}, \text{Hg}^{2+}$ and $\text{Sr}^{2+}]$ as their chloride salts and nitrate salt of Al^{3+} was used.

4.4.4. Determination of Cu^{2+} in DMSO/ H_2O (2:8, v/v) HEPES buffer solution (pH = 7.4)

The detection limit (LOD) was determined from the fluorescence titration data which is based on previously reported and broadly used methods [66–68]. Figure S14 – S17, ESI 1† reveals a good linear correlation between the concentration of Cu^{2+} ions and the value of relative fluorescence ($\Delta F = F_0 - F$) with correlation coefficient (R^2) of 0.9979. To these normalized ratio data, a linear regression curve was fitted. Then that point obtained by crossing of this line to the ordinate axis was taken as the limit of detection. The limit of detection was measured using the following formula.

$$DL = K \times \frac{\sigma}{S}$$

Where generally $K = 2$ or 3 (In this case we took $K = 3$), σ and S are the standard deviation of the blank solution and slope of the calibration curve respectively

Limit of Quantification (LOQ) was determined according to the previously reported and broadly used method [69].

$$LOQ = 10 \times \frac{\sigma}{S}$$

We have taken $K = 10$. σ and S are the standard deviation of the blank solution and slope of the calibration curve respectively.

Using the same calibration curve, linear range of concentration was also determined. Linear range of concentration is nothing but the range of concentration where the signals are directly proportional to the concentration of the analyte in the sample.

4.5. DFT calculation

All the calculations were carried out on a DFT-based geometry optimization and molecular orbital calculations were performed using the B3LYP/6-31G* functional basis set on an IBM-HS21 server cluster/LAN running in parallel with Linda, using the LINUX version of Gaussian 09 together with Gaussview 05 [70]. To avoid lengthy stages of salvation calculations of the metal chelate complexes, only excitation calculations were done in solvent to rationalize the experimentally observed solvent interactions.

The excitation calculations in DMSO solvents were done in Self-Consistent Reaction Field (SCRF) method using Polarizable Continuum Model (PCM) via the integral equation formalism variant (IEFPCM) [71].

4.6. Biological application

4.6.1. Cell culture

Human embryonic kidney 293 cell (HEK 293) line (NCCS, Pune, India) was grown in DMEM which is supplemented with FBS (10%) and antibiotics (penicillin-100 µg/ml; streptomycin-50 µg/ml). We cultured the cells at 37 °C in environment of 95% air and 5% CO₂ incubator.

4.6.2. Cell cytotoxicity assay

The 3-(4, 5-dimethylthiazol-2-yl)-2, 5-diphenyltetrazolium bromide (MTT) cell viability assay was used for the determination of cytotoxicity for ligand **L3**. We cultured HEK 293 cells (1 × 10⁵ cells/well) in a 96-well plate and incubated at just 37 °C. Then they were uncovered to varying concentrations of **L3** (1, 5, 10, 20, 40, 60, 80 and 100 µM) for nearly 24 h. When the incubation was over, then 10 µl of MTT solution [5 mg/ml, dissolved in 1X phosphate-buffered saline (PBS)] was mixed to each well of the 96-well culture plate. Then again it was incubated for just 4 h at 37 °C. We decanted media from wells and 100 µL of 0.04 N acidic isopropyl alcohol was put in into each of the well so that it can solubilize intracellular formazan crystals (blue-violet) formed and absorbance of that solution was computed at 595 nm wavelength by using EMax Precision MicroPlate Reader, Molecular Devices, USA. We have calculated values as mean ± standard errors of three independent experiments. We have expressed the cell viability was as the ratio of optical density of the treatment to control.

4.6.3. Cell imaging study

35 × 10 mm culture dish was used to culture HEK 293 Cells on coverslip for 24 h at just 37 °C. The treatment of the cells with 10 µm solution of **L3** [prepared by simple dissolution of **L3** with the mixture of two solvents DMSO: water = 2:8 (v/v)] and then it was incubated at 37 °C for 1 hour. For study of Cu²⁺ complex formation, pre-incubation of HEK 293 cells was done with 10 µM, 20 µM and 40 µM of Cu²⁺ solution for 60 min at 37 °C, after that washed three times with 1X PBS and subsequently incubated with 10µM **L3** at 37 °C for 60 min. Images of fluorescence of HEK 293 cells were captured by a fluorescence microscope (Leica DM3000, Germany) with an objective lens having 40X magnifying power.

5. Conclusion

In summary, we have revealed that this quinoline based probe is a new category of synthetic fluorescent sensor for selective recognition of Cu²⁺ ions over the other common metal ions. Also the formation of 1:1 complex for Cu²⁺ with the probe has been established by Job's plot, ESI-Mass and fluorescence data. The obtained quinoline-Cu²⁺ complex lead to the prominent fluorescence ON- OFF switching. The corresponding quenching pathway was further studied with DFT analysis and HR-MS which offered optimized structure of the complex between quinoline and Cu²⁺ ion. Moreover, the probe can be used to detect Cu²⁺ in real water samples like laboratory distilled water, tap water

and Ganges river water with a high precision and good accuracy which reaffirms the potential of the probes in various fields. In addition, this probe was further applied to fluorescence imaging for the recognition of Cu²⁺ in living HEK 293 cells. It showed less cytotoxic property and also good biocompatibility.

Declaration Of Competing Interest

There are no conflicts of interest to declare.

Acknowledgement

One of the authors (KM) wants to thank University Grants Commission (UGC) for his fellowship (SRF) and also like to thank CAS-V (UGC), DST-PURSE, DST-FIST and Department of Chemistry, University of Calcutta for supplying funds as departmental projects.

Appendix A. Supplementary data

Supplementary material related to this article can be found, in the online version, at doi:<https://doi.org/10.1016/j.jphotochem.2019.112211>.

References

- [1] Y.S. Mi, Z. Cao, Y.T. Chen, Q.F. Xie, Y.Y. Xu, Y.F. Luo, J.J. Shic, J.N. Xiang, Determination of trace amount of Cu²⁺ with a multi-responsive colorimetric and reversible chemosensor, *Analyst* 138 (2013) 5274–5280.
- [2] H. Kozłowski, A.J. Klos, J. Brasun, E. Gaggelli, D. Valensin, G. Valensin, Copper, iron, and zinc ions homeostasis and their role in neurodegenerative disorders (metal uptake, transport, distribution and regulation), *Coord. Chem. Rev.* 253 (2009) 2665–2685.
- [3] Z. Liu, W. He, M. Pei, G. Zhang, A fluorescent sensor with a detection level of pM for Cd²⁺ and nM for Cu²⁺ based on different mechanisms, *Chem. Comm.* 51 (2015) 14227–14230.
- [4] R. Uauy, M. Olivares, M. Gonzalez, Essentiality of copper in humans, *Am. J. Clin. Nutr.* 67 (1998) 952S–959S.
- [5] K.J. Barnham, C.L. Masters, A.I. Bush, Neurodegenerative diseases and oxidative stress, *Nat. Rev. Drug Discov.* 3 (2004) 205–214.
- [6] L.I. Bruijn, T.M. Miller, D.W. Cleveland, Unraveling the mechanisms involved in motor neuron degeneration in ALS, *Annu. Rev. Neurosci.* 27 (2004) 723–749.
- [7] S.H. Hahn, M.S. Tanner, D.M. Danke, W.A. Gahl, Normal metallothionein synthesis in fibroblasts obtained from children with indian childhood cirrhosis or copper-associated childhood cirrhosis, *Biochem. Mol. Med.* 54 (1995) 142–145.
- [8] D.R. Brown, H. Kozłowski, Biological inorganic and bioinorganic chemistry of neurodegeneration based on prion and Alzheimer diseases, *Dalton Trans.* (2004) 1907–1917.
- [9] D.J. Waggoner, T.B. Bartnikas, J.D. Gitlin, The role of copper in neurodegenerative disease, *Neurobiol. Dis.* 6 (1999) 221–230.
- [10] E. Gaggelli, H. Kozłowski, D. Valensin, G. Valensin, C. Homeostasis, Neurodegenerative disorders (Alzheimer's, prion, and parkinson's diseases and amyotrophic lateral sclerosis), *Chem. Rev.* 106 (2006) 1995–2044.
- [11] R.R. Nair, M. Raju, N.P. Patel, I.H. Raval, E. Suresh, S. Haldar, P.B. Chatterjee, Naked eye instant reversible sensing of Cu²⁺ and its in situ imaging in live brine shrimp *Artemia*, *Analyst* 140 (2015) 5464–5468.
- [12] K. Mal, B. Naskar, A. Mondal, S. Goswami, C. Prodhon, K. Chaudhuri, C. Mukhopadhyay, Dihydroindeno[1,2-b]pyrroles: new Al³⁺ selective off-on chemosensors for bio-imaging in living HepG2 cells, *Org. Biomol. Chem.* 16 (2018) 5920–5931.
- [13] X.H. Qian, Z.C. Xu, Fluorescence imaging of metal ions implicated in diseases, *Chem. Soc. Rev.* 44 (2015) 4487–4493.
- [14] X. Gao, C. Ding, A. Zhu, Y. Tian, Carbon-dot-Based ratiometric fluorescent probe for imaging and biosensing of superoxide anion in live cells, *Anal. Chem.* 86 (2014) 7071–7078.
- [15] L. Huang, X. Wang, G.Q. Xie, P.X. Xi, Z.P. Li, M. Xu, Y. Wu, D. Bai, Z. Zeng, A new rhodamine-based chemosensor for Cu²⁺ and the study of its behaviour in living cells, *Dalton Trans.* 39 (2010) 7894–7896.
- [16] W.Y. Liu, H.Y. Li, B.X. Zhao, J. Miao, Synthesis, crystal structure and living cell imaging of a Cu²⁺-specific molecular probe, *Org. Biomol. Chem.* 9 (2011) 4802–4805.
- [17] A. Sikdar, S.S. Panja, P. Biswas, S. Roy, A rhodamine-based dual chemosensor for Cu (II) and Fe(III), *J. Fluoresc.* 22 (2012) 443–450.
- [18] Y.J. Gong, X.B. Zhang, C.C. Zhang, A.-L. Luo, T. Fu, W. Tan, G.L. Shen, R.Q. Yu, Through bond energy transfer: a convenient and universal strategy toward efficient ratiometric fluorescent probe for bioimaging applications, *Anal. Chem.* 84 (2012) 10777–10784.
- [19] H.S. Jung, P.S. Kwon, J.W. Lee, J.I. Kim, C.S. Hong, J.W. Kim, S. Yan, J.Y. Lee, J.H. Lee, T. Joo, J.S. Kim, Coumarin-derived Cu²⁺-Selective fluorescence sensor:

- synthesis, mechanisms, and applications in living cells, *J. Am. Chem. Soc.* 131 (2009) 2008–2012.
- [20] H.S. Jung, J.H. Han, Z.H. Kim, C. Kang, J.S. Kim, Coumarin-Cu(II) ensemble-based cyanide sensing chemodosimeter, *Org. Lett.* 13 (2011) 5056–5059.
- [21] H.S. Jung, M. Park, J.H. Han, J.H. Lee, C. Kang, J.H. Jung, J.S. Kim, Selective removal and quantification of Cu(II) using fluorescent iminocoumarin-functionalized magnetic nanosilica, *Chem. Commun. (Camb.)* 48 (2012) 5082–5084.
- [22] S.P. Wu, T.H. Wang, S.R. Liu, A colorimetric and fluorescent sensor for sequential detection of copper ion and cyanide, *Tetrahedron* 70 (2014) 2822–2828.
- [23] Y. Chen, Q. Lv, Z. Liu, Q. Fang, Simple quinoline-based “turn-on” fluorescent sensor for imaging copper (II) in living cells, *Can. J. Chem.* 92 (2014) 1092–1097.
- [24] S.P. Wu, T.H. Wang, S.R. Liu, A highly selective turn-on fluorescent chemosensor for copper (II) ion, *Tetrahedron* 66 (2010) 9655–9658.
- [25] Y. Chen, Q. Lv, Z. Liu, Q. Fang, Diaminomaleonitrile substituted pyrene as a solvent-dependent chemosensor for copper(II) ion and hypochlorite, *Inorg. Chem. Commun.* 52 (2015) 38–40.
- [26] W. Shi, H. Ma, Spectroscopic probes with changeable π -conjugated systems, *Chem. Commun. (Camb.)* 48 (2012) 8732–8744.
- [27] V. Chandrasekhar, S. Das, R. Yadav, S. Hossain, R. Parihar, G. Subramaniam, P. Sen, Novel chemosensor for the visual detection of copper(II) in aqueous solution at the ppm level, *Inorg. Chem.* 51 (2012) 8664–8666.
- [28] J. Jo, H.Y. Lee, W. Liu, A. Olasz, C.H. Chen, D. Lee, Reactivity-based detection of copper(II) ion in water: oxidative cyclization of azoaromatics as fluorescence turn-on signaling mechanism, *J. Am. Chem. Soc.* 134 (2012) 16000–16007.
- [29] M.Q. Wang, K. Li, J.T. Hou, M.Y. Wu, Z. Huang, X.Q. Yu, BINOL-based fluorescent sensor for recognition of Cu(II) and sulfide anion in water, *J. Org. Chem.* 77 (2012) 8350–8354.
- [30] K. Mariappan, M. Alaparthi, G. Caple, V. Balasubramanian, M.M. Hoffman, M. Hudspeth, G.A. Sykes, Selective fluorescence sensing of copper(II) and water via competing imine hydrolysis and alcohol oxidation pathways sensitive to water content in aqueous acetonitrile mixtures, *Inorg. Chem.* 53 (2014) 2953–2962.
- [31] J.H. Jang, S. Bhuniya, J. Kang, A. Yeom, K.S. Hong, J.S. Kim, Cu²⁺-Responsive bimodal (Optical/MRI) contrast agent for cellular imaging, *Org. Lett.* 15 (2013) 4702–4705.
- [32] Y.H. Lee, N. Park, Y.B. Park, Y.J. Hwang, C. Kang, J.S. Kim, Organelle-selective fluorescent Cu²⁺ ion probes: revealing the endoplasmic reticulum as a reservoir for Cu-overloading, *Chem. Commun. (Camb.)* 50 (2014) 3197–3200.
- [33] X. Liu, Y. Li, X. Ren, Q. Yang, Y. Su, L. Hea, X. Song, Methylated chromenoquinoline dyes: synthesis, optical properties, and application for mitochondrial labeling, *Chem. Commun. (Camb.)* 54 (2018) 1509–1512.
- [34] B. Zhang, F. Qin, H. Niu, Y. Liu, D. Zhang, Y. Ye, A highly sensitive and fast responsive naphthalimide-based fluorescent probe for Cu²⁺ and its application, *New J. Chem.* 41 (2017) 14683–14688.
- [35] S. Li, D. Zhang, X. Xie, S. Ma, Y. Liu, Z. Xu, Y. Gao, Y. Ye, A novel solvent-dependently bifunctional NIR absorptive and fluorescent ratiometric probe for detecting Fe³⁺/Cu²⁺ and its application in bioimaging, *Sens. Actuators B Chem.* 224 (2016) 661–667.
- [36] L. Wang, B. Chen, P. Peng, W. Hu, Z. Liu, X. Pei, W. Zhao, C. Zhang, L. Li, W. Huang, Fluorescence imaging mitochondrial copper(II) via photocontrollable fluorogenic probe in live cells, *Chin. Chem. Lett.* 28 (2017) 1965–1968.
- [37] J. Tang, S. Ma, D. Zhang, Y. Liu, Y. Zhao, Y. Ye, Highly sensitive and fast responsive ratiometric fluorescent probe for Cu²⁺ based on a naphthalimide-rhodamine dyad and its application in living cell imaging, *Sens. Actuators B Chem.* 236 (2016) 109–115.
- [38] C.J. Gao, X.J. Jin, X.H. Yan, P. An, Y. Zhang, L.L. Liu, A small molecular fluorescent sensor for highly selectivity of zinc ion, *Sens. Actuators B Chem.* 176 (2013) 775–781.
- [39] Y. Weng, Z.L. Chen, F. Wang, L. Xue, H. Jiang, High sensitive determination of zinc with novel water-soluble small molecular fluorescent sensor, *Anal. Chim. Acta* 647 (2009) 215–218.
- [40] X.M. Meng, S.X. Wang, Y.M. Li, M.Z. Zhu, Q.X. Guo, 6-Substituted quinoline-based ratiometric two-photon fluorescent probes for biological Zn²⁺ detection, *Chem. Commun. (Camb.)* 48 (2012) 4196–4198.
- [41] H. Liu, Y. Dong, B. Zhang, F. Liu, C. Tan, Y. Tan, An efficient quinoline-based fluorescence sensor for zinc(II) and its application in live-cell imaging, *Sens. Actuators B Chem.* 234 (2016) 616–624.
- [42] L. Xu, M.L. He, H.B. Yang, X. Qian, A simple fluorescent probe for Cd²⁺ in aqueous solution with high selectivity and sensitivity, *Dalton Trans.* 42 (2013) 8218–8222.
- [43] X. Su, T.F. Robbins, I. Arahamian, Switching through coordination-coupled proton transfer, *Angew. Chem. Int. Ed.* 50 (2011) 1841–1844.
- [44] A. Chakraborty, S. Kar, D.N. Nath, N. Guchhait, Photoinduced intramolecular charge transfer reaction in (*E*)-3-(4-Methylamino-phenyl)-acrylic acid methyl ester: a fluorescence study in combination with TDFT calculation, *J. Phys. Chem. A* 110 (2006) 12089–12095.
- [45] B.K. Paul, A. Samanta, S. Kar, N. Guchhait, Evidence for excited state intramolecular charge transfer reaction in donor-acceptor molecule 5-(4-dimethylamino-phenyl)-penta-2,4-dienoic acid methyl ester: experimental and quantum chemical approach, *J. Lumin.* 130 (2010) 1258–1267.
- [46] A. Mallick, M.C. Mandal, B. Haldar, A. Chakraborty, P. Das, N. Chattopadhyay, Surfactant-induced modulation of fluorosensor activity: a simple way to maximize the sensor efficiency, *J. Am. Chem. Soc.* 128 (2006) 3126–3127.
- [47] K. Mal, S. Chatterjee, A. Bhaumik, C. Mukhopadhyay, Mesoporous MCM-41 silica supported pyridine nanoparticle: a highly efficient, recyclable catalyst for expeditious synthesis of quinoline derivatives through domino approach, *ChemistrySelect* 4 (2019) 1776–1784.
- [48] C. Zhou, H. Liu, Y. Zhang, A novel quinoline-based fluorescent sensor for imaging Copper (II) in living cells, *Main Group Chem.* 17 (2018) 53–61.
- [49] A. Mondal, B. Naskar, S. Goswami, C. Prodhon, K. Chaudhuri, C. Mukhopadhyay, 12 catalyzed access of spiro[indoline-3,4'-pyridine] appended amine dyad: new ON-OFF chemosensors for Cu²⁺ and imaging in living cells, *Org. Biomol. Chem.* 16 (2018) 302–315.
- [50] N. Roy, S. Nath, A. Dutta, P. Mondal, P.C. Paul, T.S. Singh, A highly efficient and selective coumarin based fluorescent probe for colorimetric detection of Fe³⁺ and fluorescence dual sensing of Zn²⁺ and Cu²⁺, *RSC Adv.* 6 (2016) 63837–63847.
- [51] S. Pathak, D. Das, A. Kundu, S. Maity, N. Guchhait, A. Pramanik, Synthesis of 4-hydroxyindole fused isocoumarin derivatives and their fluorescence “Turn-off” sensing of Cu(II) and Fe(III) ions, *RSC Adv.* 5 (2015) 17308–17318.
- [52] Y. Gao, J. Shua, C. Zhang, X. Zhang, H. Cheng, K. Yao, A fluorescence on-off sensor for Cu²⁺ and its resultant complex as an off-on sensor for Cr³⁺ in aqueous media, *RSC Adv.* 5 (2015) 74629–74637.
- [53] S. Erdemir, B. Tabakci, M. Tabakci, A highly selective fluorescent sensor based on calix[4]arene appended benzothiazole units for Cu²⁺, S²⁻ and HSO₄⁻ ions in aqueous solution, *Sens. Actuators B Chem.* 228 (2016) 109–116.
- [54] P. Puangploya, S. Smanmoob, W. Surareungchai, A new rhodamine derivative-based chemosensor for highly selective and sensitive determination of Cu²⁺, *Sens. Actuators B Chem.* 193 (2014) 679–686.
- [55] G. Xua, J. Wang, G. Si, M. Wang, X. Xue, B. Wu, S. Zhou, A novel highly selective chemosensor based on curcumin for detection of Cu²⁺ and its application for bioimaging, *Sens. Actuators B Chem.* 230 (2016) 684–689.
- [56] Y. Fang, Y. Zhou, Q. Rui, C. Yao, Rhodamine-ferrocene conjugate chemosensor for selectively sensing copper(II) with multisignals: chromaticity, fluorescence, and electrochemistry and its application in living cell imaging, *Organometallics* 34 (2015) 2962–2970.
- [57] Y. Fu, Q.C. Feng, X.J. Jiang, H. Xu, M. Lia, S.Q. Zang, New fluorescent sensor for Cu²⁺ and S²⁻ in 100 % aqueous solution based on displacement approach, *Dalton Trans.* 43 (2014) 5815–5822.
- [58] M.-Q. Wang, K. Li, J.-T. Hou, M.-Y. Wu, Z. Huang, X.-Q. Yu, BINOL-based fluorescent sensor for recognition of Cu(II) and sulfide anion in water, *J. Org. Chem.* 77 (2012) 8350–8354.
- [59] B.R. White, J.A. Holcombe, Fluorescent peptide sensor for the selective detection of Cu²⁺, *Talanta* 71 (2007) 2015–2020.
- [60] W. Yang, X. Chen, H. Su, W. Fang, Y. Zhang, The fluorescence regulation mechanism of the paramagnetic metal in a biological HNO sensor, *Chem. Commun. (Camb.)* 51 (2015) 9616–9619.
- [61] SMART, SAINT Software Reference Manuals 6 Bruker Analytical X-ray Systems, Inc., Madison, WI, 2003 45.
- [62] G.M. Sheldrick, SADABS, A Software for Empirical Absorption Correction 2 University of Göttingen: Göttingen, Germany, 2002 05.
- [63] SHELXTL Reference Manual 6 Bruker Analytical X-ray Systems, Inc., Madison, WI, 2000 1.
- [64] G.M. Sheldrick, SHELXTL 6 Bruker AXS, Inc., Madison, WI, 2001 12.
- [65] G.M. Sheldrick, A short history of SHELX, *Acta Crystallogr.* 64 Sect. A: Fundam. Crystallogr., 2008, pp. 112–122.
- [66] B. Naskar, R. Modak, D.K. Maiti, A. Bauzá, A. Frontera, P.K. Maiti, S. Mandal, S. Goswami, A highly selective “ON-OFF” probe for colorimetric and fluorometric sensing of Cu²⁺ in water, *RSC Adv.* 7 (2017) 11312–11321.
- [67] A. Caballero, R. Martínez, V. Lloveras, I. Ratera, J. Vidal-Gancedo, K. Wurst, A. Tárraga, P. Molina, J. Veciana, Highly Selective Chromogenic and Redox or Fluorescent Sensors of Hg²⁺ in Aqueous Environment Based on 1,4-Disubstituted Azines, *J. Am. Chem. Soc.* 127 (2005) 15666–15667.
- [68] L.R. Romo, M.T.O. Guzman, A.O. Sarabia, G.P. Luis, Flavone functionalized magnetic nanoparticles: a new fluorescent sensor for Cu²⁺ ions with nanomolar detection limit, *Sens. Actuators B Chem.* 233 (2016) 459–468.
- [69] A. Shrivastava, V.B. Gupta, Methods for the determination of limit of detection and limit of quantitation of the analytical methods, *Chron. Young Sci.* 2 (2011) 21–25.
- [70] M.J. Frisch, G.W. Trucks, H.B. Schlegel, G.E. Scuseria, M.A. Robb, J.R. Cheeseman, G. Scalmani, V. Barone, G.A. Petersson, H. Nakatsuji, X. Li, M. Caricato, A. Marenich, J. Bloino, B.G. Janesko, R. Gomperts, B. Mennucci, H.P. Hratchian, J.V. Ortiz, A.F. Izmaylov, J.L. Sonnenberg, D. Williams-Young, F. Ding, F. Lipparini, F. Egidi, J. Goings, B. Peng, A. Petrone, T. Henderson, D. Ranasinghe, V.G. Zakrzewski, J. Gao, N. Rega, G. Zheng, W. Liang, M. Hada, M. Ehara, K. Toyota, R. Fukuda, J. Hasegawa, M. Ishida, T. Nakajima, Y. Honda, O. Kitao, H. Nakai, T. Vreven, K. Throssell, J.A. Montgomery Jr., J.E. Peralta, F. Ogliaro, M. Bearpark, J.J. Heyd, E. Brothers, K.N. Kudin, V.N. Staroverov, T. Keith, R. Kobayashi, J. Normand, K. Raghavachari, A. Rendell, J.C. Burant, S.S. Iyengar, J. Tomasi, M. Cossi, J.M. Millam, M. Klene, C. Adamo, R. Cammi, J.W. Ochterski, R.L. Martin, K. Morokuma, O. Farkas, J.B. Foresman, D.J. Fox, Gaussian 09, Revision A.02, Gaussian, Inc., Wallingford CT, 2016.
- [71] A.V. Marenich, C.J. Cramer, D.G. Truhlar, Universal solvation model based on solute electron density and a continuum model of the solvent defined by the bulk dielectric constant and atomic surface tensions, *J. Phys. Chem. B* 113 (2009) 6378–96.